Identifying Tire Pressure Variation by Nonlinear Estimation of Longitudinal Stiffness and Effective Radius

Christopher R. Carlson
Stanford University
Mechanical Engineering
Stanford, CA 94305-4021, USA
crcarlson@stanford.edu

J. Christian Gerdes
Stanford University
Mechanical Engineering
Stanford, CA 94305-4021, USA
gerdes@cdr.stanford.edu

Previous work estimates longitudinal stiffness and wheel effective radius using a linear least squares estimator and GPS as an absolute velocity sensor. This paper extends this work by reformulating the problem with an energy interpretation and demonstrates that both linear formulations are sensitive to small values of measurement noise with a simulation study. It then proposes two nonlinear estimation schemes which appear to be unbiased when subjected to observed levels of measurement noise in truth simulations. These nonlinear schemes are then applied to real test vehicle data and predict that as tire pressure decreases by $\sim 10\%$, longitudinal stiffness increases by $\sim 10\%$. This apparent sensitivity suggests that any force-slip analysis must carefully control tire pressure before any conclusions about tire properties can be made. It also suggests that a longitudinal stiffness estimate may be used to predict tire inflation pressure.

Keywords/ least squares, estimation, longitudinal stiffness, slip, tire, effective radius, GPS

1 INTRODUCTION

The SAE definition for wheel slip is:

$$\text{Slip} \quad = \quad -\left(\frac{V - R\omega}{V}\right) \tag{1}$$

Where V is the velocity of the center of the tire, R is the effective radius of the tire and ω is angular velocity of the tire. Empirical tire models such as the Magic Formula [3] model the relationship between force transmitted by the tire and the resulting slip with complicated nonlinear relationships. Figure 1 shows typical force-slip curves of the Magic Formulae for different values of road surface to tire friction. A

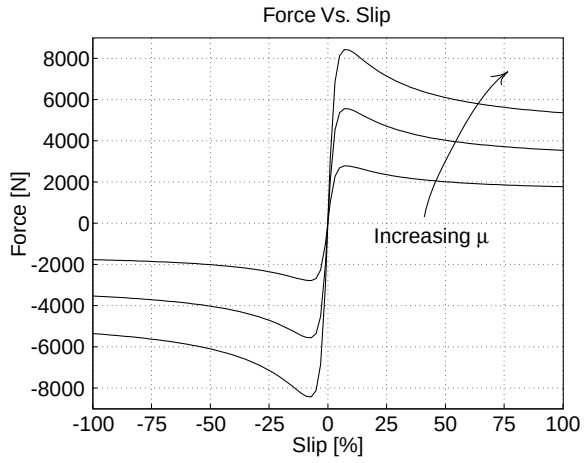

Figure 1: Magic Formula tire model curves for increasing μ

common trend among tire models is that for tire slip below about 3%, the relationship between force and slip is approximately linear. In this linear region, the force slip relation can be characterized as:

$$F \quad = \quad C_x\left(\frac{V - R\omega}{V}\right) \tag{2}$$

Where F and C_x are the force and longitudinal stiffness of the tire(s) transmitting the force.

Up until recently it has been difficult to measure absolute vehicle velocity accurately. Inertial measurement based observers were proposed in [4]. Work in [6] and [10] discuss the advantages of using Global Positioning System (GPS) velocity as an absolute velocity sensor for measuring slip. While GPS could be used directly, this paper assumes the vehicle is front wheel drive and that the rear wheels are free to roll at all times. Absolute vehicle velocity is calculated by first identifying the rear wheel free rolling radius to sub-millimeter accuracy using GPS; vehicle velocity is then calculated by multiplying the identified tire radius by the wheel speed measurement similar to the work in [8].

Several research groups propose that tire longitudinal stiffness at low values of slip may indicate the tire to road friction coefficient and thus the peak value of the force slip curve [4],[8],[9],[11]. This paper shows that longitudinal stiffness estimates exhibit considerable sensitivity to tire inflation pressure. Empirical studies in [12] suggest that tire pressure decrease of $\sim 10\%$ should yield a $\sim 10\%$ stiffness increase, while only a $\sim 3\%$ increase in peak friction force. This sophisticated dependence of tire behaviors upon (possibly unknown) tire parameters such as inflation pressure suggests that any force-slip analysis must carefully consider a variety of factors before drawing any conclusions about tire properties.

In the TREAD Act of November 1, 2000, Congress required the National Highway Traffic Safety Administration (NHTSA) to develop a rule requiring all new motor vehicles to be equipped with a warning system to indicate to the operator when a tire is significantly underinflated [7]. The nonlinear algorithms described in this paper are able to (under controlled conditions) detect tire pressure variation of the front wheels to $\sim 5\%$. Further modeling of individual tire braking forces may produce an algorithm capable of estimating all four wheel pressures with only a GPS receiver and stock automotive sensors.

This paper continues previous work in [10] by first reinterpreting the force balance in equation 2 as an energy balance. A truth simulation goes on to show that both the regression in [10] and the new formulation are extremely sensitive to measurement noise. In the spirit of least squares estimation, these problems are then reformulated into nonlinear forms which seek to minimize the measurement errors and not the equation errors. A heuristic for solving the nonlinear estimation problems is presented and its feasibility is demonstrated with truth simulations. Finally the algorithms are run on vehicle test data and they suggest tire pressure and longitudinal stiffness are approximately inversely proportional near the designed operating pressure as noted in [12] and suspected in [10]. Thus, a robust longitudinal stiffness estimate may serve as a tire pressure indicator.

2 REVIEW OF LEAST SQUARES

Following sections are inspired by the assumptions of least squares estimation in a non-obvious way. As such the assumptions of least squares are reviewed here.

A least squares estimator seeks to minimize the sum of the squared equation errors. This makes sense when the errors tend to be independent, zero mean (IZM) and enter the equation with the measurement vector y. This idea is equivalent the following optimization problem:

$$\begin{array}{rl} \text{Minimize} & \|\Delta y\|_2 \\ \text{subject to:} & y = f(\theta) + \Delta y \end{array}$$

Where $f(\theta)$ is the system model and Δy is the measurement error. When $f(\theta)$ represents a linear function of the parameters θ, it can be written:

$$y = A\theta + \Delta y$$

where A is a matrix. When there are more measurements than unknowns, this problem has a quadratic cost function with the familiar analytical solution:

$$\begin{aligned} \hat{\theta} &= (A'A)^{-1}A'y \\ &= A^{\dagger}y \end{aligned}$$

The bias of this estimator can be understood statistically by looking at the expected value (E) of the parameter estimates:

$$\begin{aligned} E(\hat{\theta}) &= E(A^{\dagger}y) \\ &= E(A^{\dagger}(A\theta + \Delta y)) \\ &= \theta + E(A^{\dagger}\Delta y)) \end{aligned}$$

from this last equation it is clear that Δy must be uncorrelated with $A^{\dagger}$ and zero mean for the parameter estimate $\hat{\theta}$ to be unbiased. One way to interpret this result is that minimizing the sum of the squared measurement errors will return the true parameter estimates when the errors are IZM and uncorrelated with the regressors in A.

3 LINEAR FORMULATIONS

3.1 Linear Force Form

Previous work in [10] attempted to estimate the driven tire parameters C_x and R_f by formulating equation 2 as a linear regression:

$$\hat{a} = \begin{bmatrix} -\frac{1}{m} & \frac{\hat{\omega}_f}{m\hat{V}} \end{bmatrix} \begin{bmatrix} C_x \\ R_f C_x \end{bmatrix} \quad (3)$$

Where m is the mass of the vehicle and $\hat{a}, \hat{\omega}_f, \hat{V}$ represent vehicle acceleration, front wheel angular velocity and vehicle velocity. The $\hat{hat}$ notation represents measured values or values calculated from measurements. One way to interpret this formulation is that the estimator is seeking to minimize the force error in the least squares sense, which is not the same as minimizing the measurement errors. With measurement perturbations the equation becomes:

$$a + \Delta a = \begin{bmatrix} -\frac{1}{m} & \frac{\omega_f + \Delta\omega_f}{m(V+\Delta V)} \end{bmatrix} \begin{bmatrix} C_x \\ R_f C_x \end{bmatrix} \quad (4)$$

Where the Δ parameters represent measurement perturbations. Rearranging the deterministic and stochastic parts:

$$\begin{aligned} a - \begin{bmatrix} -\frac{1}{m} & \frac{\omega_f}{mV} \end{bmatrix} \begin{bmatrix} C_x \\ R_f C_x \end{bmatrix} = \\ -\Delta a + \begin{bmatrix} 0 & \Delta\left(\frac{\omega_f}{mV}\right) \end{bmatrix} \begin{bmatrix} C_x \\ R_f C_x \end{bmatrix} \end{aligned} \quad (5)$$

where,

$$\Delta\left(\frac{\omega_f}{mV}\right) = \frac{V\Delta\omega_f - \omega_f\Delta V}{m(V+\Delta V)V} \quad (6)$$

Although linear in the parameters, the above estimation scheme violates other assumptions of least squares. The value $\hat{a}$ was estimated by numerically differentiating measurements from GPS velocity:

$$\begin{aligned} \hat{a}^k &\cong \frac{\hat{V}^{k+1} - \hat{V}^{k-1}}{2T} \\ &= \frac{V^{k+1} - V^{k-1}}{2T} + \frac{\Delta V^{k+1} - \Delta V^{k-1}}{2T} \\ &= a^k + \Delta a^k \end{aligned}$$

In general, the time derivative of the IZM random variable, $\Delta\dot{V}^k \triangleq \Delta a^k$, is not IZM since it is necessarily correlated with itself in time. Likewise the front

wheel angular velocity $\hat{\omega}_f$ above was estimated by differentiating wheel angle measurements. Thus the equation error for the above formulation is not IZM which leads to parameter bias from a least squares estimator.

The above scheme also includes implicit regularization by incorporating measurements in the second column of the estimation matrix. Explicitly separating the noise terms from the measurements as in equation 5 shows how the multiplicative $\Delta\left(\frac{\omega_f}{mV}\right)$ errors will tend to bias the parameter estimates. The larger the $R_f C_x$ parameter, the larger the noise contribution from the measurement error in the second column becomes. Since least squares seeks to minimize the equation error, this will tend to encourage the estimator to make the parameter $R_f C_x$ small.

Although the structure in equation 3 seems reasonable, this section has shown that it will tend to yield biased parameter estimates. A subsequent section demonstrates these biases can be quite large for small measurement noise values with truth simulations. Clearly if this scheme fails for simplified simulated experiments, it is highly unlikely that it will perform better for real data.

3.2 Linear Energy Form

Equation 3 may be rewritten with an energy interpretation such that the differentiation of θ_f to obtain ω_f is unnecessary:

$$\begin{aligned} m\frac{dV}{dt} &= -C_x\left(\frac{V-R\omega}{V}\right) \\ m\int V dV &= -C_x\int (V-R\omega)dt \\ mV^2 - mV_0^2 &= -2C_x(S-R\theta) \end{aligned}$$

This equation equates the kinetic energy added to the vehicle to the longitudinal stiffness multiplied by the slipped distance of the drive tire.

For this investigation, vehicle velocity V is measured as:

$$V = R_r\dot{\theta}_r \tag{7}$$

where R_r is the rear wheel free-rolling radius and θ_r is rear wheel angular displacements measured by an ABS variable reluctance sensor. R_r is assumed constant and is estimated separately using GPS.

Substituting equation 7 into the energy equation above and letting θ_f, R_f be the front wheel angle and radius respectively yields:

$$mR_r^2\left(\dot{\theta_r}^2 - \dot{\theta_{r0}}^2\right) = -2C_x(R_r\theta_r - R_f\theta_f) \tag{8}$$

Which assumes that the front wheel provides all the force on the vehicle and the rear wheel always stays free to roll.

Once again approximating the time derivatives as finite difference equations and forming a linear regression similar to equation 3.

$$mR_r^2\left(\dot{\hat{\theta}_r}^2 - \dot{\hat{\theta}_{r0}}^2\right) = -2\begin{bmatrix} R_r\hat{\theta}_r & -\hat{\theta}_f \end{bmatrix}\begin{bmatrix} C_x \\ R_f C_x \end{bmatrix}$$

This formulation generates more consistent, although biased estimates of the parameters in simulation. The bias is not surprising since once again our measurement errors are not IZM and the estimation structure still implicitly weights the residuals by including measurements in the estimation matrix. The following section details the truth simulation for these estimation schemes.

3.3 Linear Truth Simulation

A continuous simulation models the force, velocity and slip using equation 1. All other dynamics such as vehicle pitch and tire deformation are ignored. The errors of the wheel angular displacement signals are modeled as white noise which is added to the simulated sensor measurements. Typical standard deviations used to model the noise of the wheelspeed measurements is $0.04[rad]$ which is less than the resolution of the wheel angle sensor $[100counts/rev]$. The simulated vehicle accelerates at $3[m/s^2]$ and decelerates at $-1[m/s^2]$ for times which yield an average velocity of $13[m/s]$. These accelerations are physically realizable by our test vehicle and were chosen to mimic accelerations and velocities during data collection conditions which appear later in this paper. Figure 2 demonstrates a representative set of simulation data.

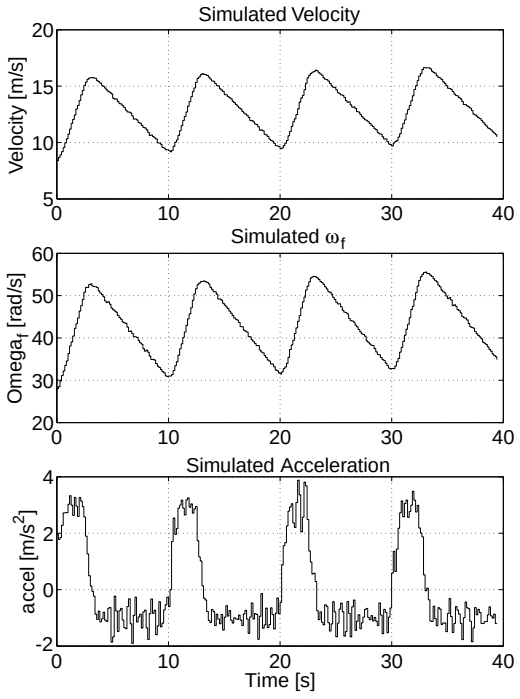

Figure 2: Typical truth simulation velocity, ω_f and acceleration

Figure 3 illustrates parameter estimation results of twenty simulated data sets. The force formulation consistently underestimates the longitudinal stiffness

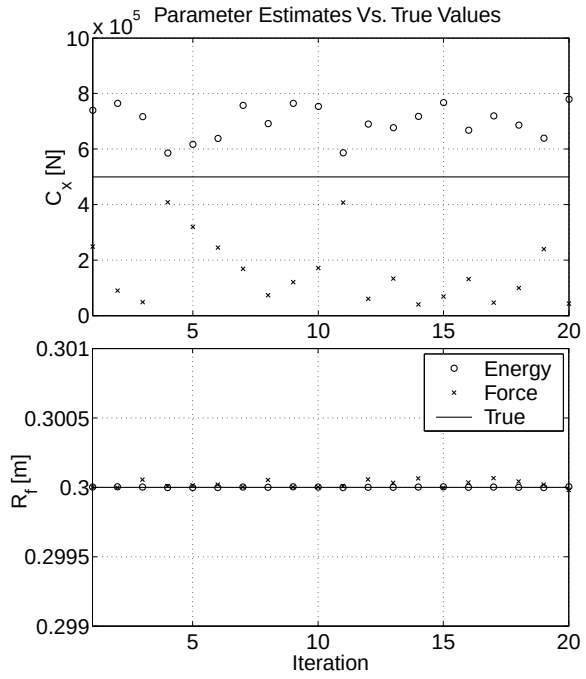

Figure 3: Truth simulation for linear parameter estimation schemes

by about a factor of 5, while the energy form tends to over estimate the stiffness by about 50%. It is interesting to note that the wheel radius is consistently estimated to sub millimeter accuracy by both linear estimation schemes.

4 NONLINEAR FORMULATIONS

In the spirit of a least squares solution, the following optimization problems seek to minimize the *measurement errors*, which in these formulations are not the same as the equation errors. Although the solutions to these problems are more difficult to compute, the resulting parameter estimates appear to be unbiased.

4.1 Nonlinear Force Form

Introducing measurement noise perturbations into equation 2 yields:

$$mR_r(\theta_r + \ddot{\Delta\theta_r}) = -C_x\left(\frac{R_r(\theta_r + \dot{\Delta\theta_r}) - R_f(\theta_f + \dot{\Delta\theta_f})}{R_r(\theta_r + \dot{\Delta\theta_r})}\right)$$

Moving everything to the left hand side,

$$mR_r^2(\theta_r + \ddot{\Delta\theta_r})(\theta_r + \dot{\Delta\theta_r}) + C_x\left(R_r(\theta_r + \dot{\Delta\theta_r}) - R_f(\theta_f + \dot{\Delta\theta_f})\right) = 0 \quad (9)$$

The solution to these problems will be iterative and the time derivatives are approximated by first order finite difference equations. Let each measurement be written as:

$$\hat{\theta}^k = \theta^k + \Delta\theta^k$$

then,

$$\dot{\hat{\theta}}^k \cong \frac{\hat{\theta}^{k+1} - \hat{\theta}^{k-1}}{2T} \quad (10)$$

$$\ddot{\hat{\theta}}^k \cong \frac{\hat{\theta}^{k+2} - 2\hat{\theta}^k + \hat{\theta}^{k-2}}{4T^2} \quad (11)$$

where k represents the discrete time step and T represents the digital sampling rate. Equation 9 can be written more conveniently as:

$$f^k(\hat{\theta}_r, \hat{\theta}_f, \Delta\theta_r, \Delta\theta_f, R_f, C_x) = 0$$

The goal of minimizing the sum of the squared measurement errors, which should yield the correct parameter estimates in the presence of IZM noise, can then be stated:

$$\begin{aligned} &\text{Minimize: } \|\Delta\theta_r; \Delta\theta_f\| \\ &\text{Subject to: } f^k(\hat{\theta}_r, \hat{\theta}_f, \Delta\theta_r, \Delta\theta_f, R_f, C_x) = 0 \end{aligned} \quad (12)$$

4.2 Nonlinear Energy Form

As above, introduce measurement noise perturbations into equation 8:

$$mR_r^2(\theta_r + \dot{\Delta\theta_r})^2 - mR_r^2(\theta_{r0} + \dot{\Delta\theta_{r0}})^2 = -2C_x(R_r(\theta_r + \Delta\theta_r) - R_f(\theta_f + \Delta\theta_f))$$

Which can be written as

$$mR_r^2(\theta_r + \dot{\Delta\theta_r})^2 - mR_r^2(\theta_{r0} + \dot{\Delta\theta_{r0}})^2 + 2C_x(R_r(\theta_r + \Delta\theta_r) - R_f(\theta_f + \Delta\theta_f)) = 0$$

Using the same time derivative approximation for the $\dot{\hat{\theta}}$ terms in equation 10, the above equation can be written:

$$g^k(\hat{\theta}_r, \hat{\theta}_f, \Delta\theta_r, \Delta\theta_f, R_f, C_x) = 0$$

Then, the goal of minimizing the sum of the squared measurement errors is stated:

$$\begin{aligned} &\text{Minimize: } \|\Delta\theta_r; \Delta\theta_f\| \\ &\text{Subject to: } g^k(\hat{\theta}_r, \hat{\theta}_f, \Delta\theta_r, \Delta\theta_f, R_f, C_x) = 0 \end{aligned} \quad (13)$$

4.3 Nonlinear Solution Computation

Like the unbiased estimator in equation 3, these solutions seek to minimize the sensor errors. Unlike equation 3, these problems do not have analytical solutions. In this paper, they are solved heuristically by searching the parameter space of C_x, R_f until the $\min_{C_x,R_f}(min(\|\Delta\theta_r; \Delta\theta_f\|))$ is found. As with least squares, the C_x and R_f which minimize $\min_{C_x,R_f}(min(\|\Delta\theta_r; \Delta\theta_f\|))$ should be the true parameters.

For each candidate value of C_x, R_f, $min(\|\Delta\theta_r; \Delta\theta_f\|)$ is a nonlinear minimum norm problem, the dual of nonlinear least squares. The minimum norm solution is iterative and a typical solution using a Gauss-Newton solver progresses as in figure 4. Recall that a minimum norm

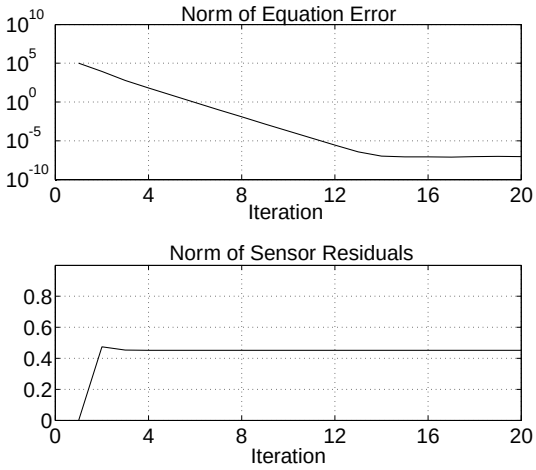

Figure 4: Typical convergence of minimum norm solution

problem seeks a set of parameters which cause an underdetermined set of equations to equal zero. For this nonlinear solver, the magnitude of the parameters converges after only a few iterations while the actual solution converges (to zero) much more slowly. Even though, for low iterations, the solution to the equation does not yet equal zero, the parameters which are minimized are not decreasing in magnitude. The estimators in this paper seek to minimize the magnitude of the parameters. Iterating on the exact nonlinear solution does not yield any more information. This suggests that the stopping criteria should be placed on the variation in residual magnitude and not on the usual stopping condition which is the norm of the equation error.

Once a minimum norm solution for a particular C_x and R_f is computed, one then minimizes $min(\|\Delta\theta_r; \Delta\theta_f\|)$ across the parameter space of C_x and R_f. Although this methodology does not in general guarantee a global minimum norm solution to equations 12 & 13, so far simulation and data have always yielded quasi-convex cost functions of C_x, R_f as per figures 5 and 6 which are globally solved by bisection.

4.4 Nonlinear Truth Simulation

The above algorithms, run on the same truth simulation as in the linear case in figure 3, yield estimates for C_x and R_f in figure 7. The nonlinear energy and force form parameter estimates consistently estimate the longitudinal stiffness to within about 2% or 3% for data sets on the order of 600 points long. Front wheel radius is always estimated within $5 \times 10^{-6}[m]$ This accuracy of the estimate R_f is reflected in the cost function in figures 5 and 6. A deviation of 0.05% in the radius estimate costs the same as a deviation of 50% to more than 100% in the longitudinal stiffness estimate depending on which side of the cost surface the solution is on. Specifically this means that a $0.1[mm]$ variation in front tire radius estimate could yield as much as $2.5 \times 10^5[N]$ variation in longitudinal stiffness estimate. In some sense these cost sensitivities represent the difficulties of obtaining good parameter estimates. Measuring wheel radius is a simple matter of dividing the length of path traveled by the number of revolutions of the tire, while measuring wheel slip involves measuring the difference in wheel rotations between the front and rear wheels to a small fraction of one percent.

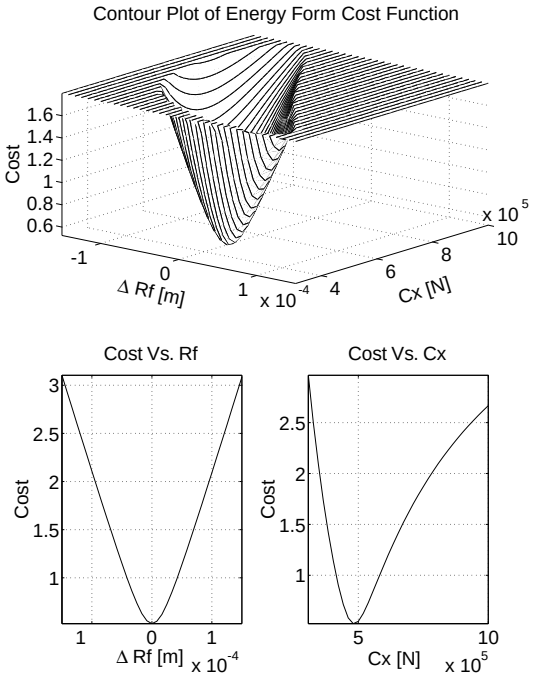

Figure 5: Typical cost function for energy formulation and cross sections

The residuals for these nonlinear estimation schemes tend to underestimate the magnitude of the noise. Figure 8 shows histogram plots of the simulation noise and the calculated residuals using the energy formulation. The calculated residuals tend to be approximately 75% the magnitude of the noise magnitudes. The force formulation yields similar residual histograms which also underestimate the magnitude of the sensor noise by about 25%.

5 EXPERIMENTAL RESULTS

5.1 Experimental Setup

All data analyzed in the following section was recorded on a 1998 Ford Windstar minivan with stock installed variable reluctance Antilock Braking System (ABS) sensors. Additional equipment includes a Novatel GPS receiver and a Versalogic single board computer running the MATLAB XPC embedded realtime operating system. This system records and processes 20 data streams comfortably at sample rates up to 1000 hz.

Tires are very complex components with time varying properties which change on the order of seconds to hours of use. In an effort to hold as many tire variables constant as possible, the data collected for these results were collected on the same section of

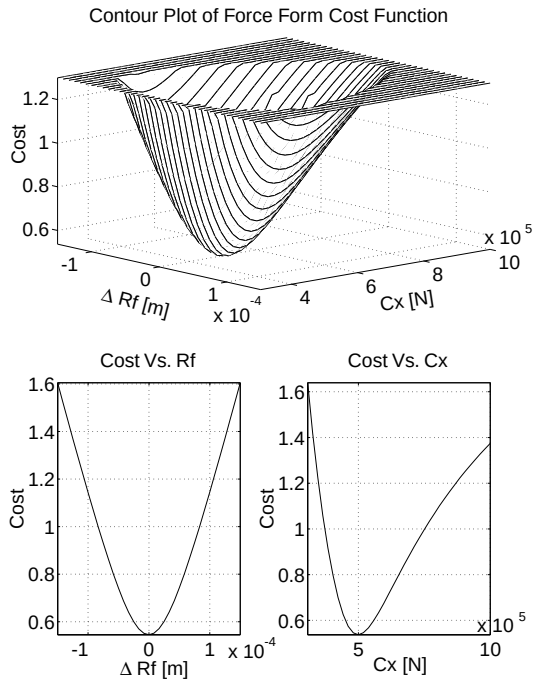

Figure 6: Typical cost function for force formulation and cross sections

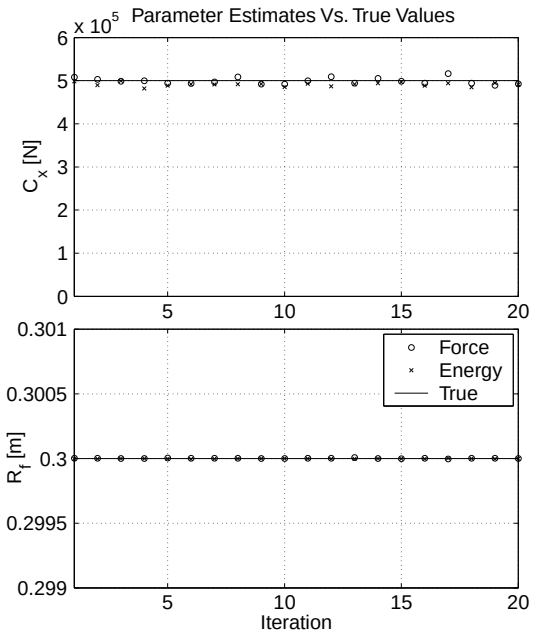

Figure 7: Truth Simulation for nonlinear parameter estimation schemes

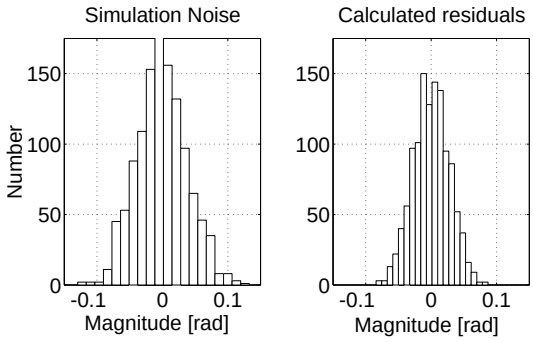

Figure 8: Histograms of truth simulation noise and estimation residuals

asphalt on a nearly flat, straight, dry, road about 1 mile long to eliminate the effects of turning and road grade as much as possible from the measurements. Force was applied to the tires by accelerating with throttle and decelerating with engine braking only. Thus the rear wheels were free to roll at all times. The test road has no overhanging trees or tall buildings nearby so the GPS antenna had an unobstructed view of sky and was unlikely to experience multipath errors. The nominal air temperature was $12^{\circ}[C]$ and the tires were allowed to cool to a nominal temperature with 4 minutes of low force driving between each data set. Front tire pressures were measured and adjusted at normal driving temperature. Wheel angular displacements were recorded at 100Hz, summed over the length of the data set and then sub-sampled at 10Hz to reduce the auto correlation of high frequency wheel modes and reduce the computational cost of the nonlinear solution. Thus data sets are on the order of 900 points long. A typical data set appears in figure 9.

5.2 Data Analysis

The above algorithm, run on 15 separate data sets each about 90 seconds long, produces the following estimates of longitudinal stiffness and front wheel radius in figure 10. C_x here refers to the combined longitudinal stiffness of both front tires as the transmission differential will average the force applied. Runs $[1-5]$ were taken at $252[kPa]$, runs $[6-10]$ at $221[kPa]$ and runs $[11-15]$ at $200[kPa]$. A 10 percent variation in tire pressure generally yielded a 10 percent increase in longitudinal stiffness which is consistent with the trends noted by [12]. The physical interpretation of this variation is that lowering the tire pressure will tend to increase the area of the contact patch of the tire. The resulting increased contact area of the tire will then tend to slide less for the same force which causes the stiffness to go up.

As suggested by the gradients of the cost functions, the front tire effective radius shows very little variation across trials at the same pressure. Here the radius estimates vary on the order of $1 \times 10^{-5}[m]$.

Figure 11 is a typical histogram for experimental data estimation residuals $\Delta\theta_f$, $\Delta\theta_r$, when R_f and C_x are chosen according to the energy formulation algorithm. This shape appears to be the sum of two gaussian distributions with mean of $\pm 0.025[rad]$. This bimodal distribution implies the estimates may be biased due to unmodeled behavior. However, nearly all of the residuals are still under $0.05[rad]$ which is the resolution of the variable reluctance sensor used to measure wheel angular displacement. The low residual magnitudes suggest that the bias is probably not extremely large.

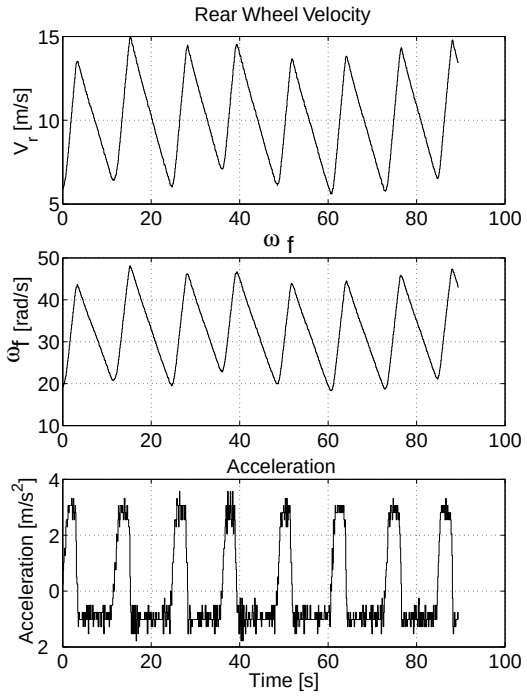

Figure 9: A typical data set for longitudinal stiffness estimation

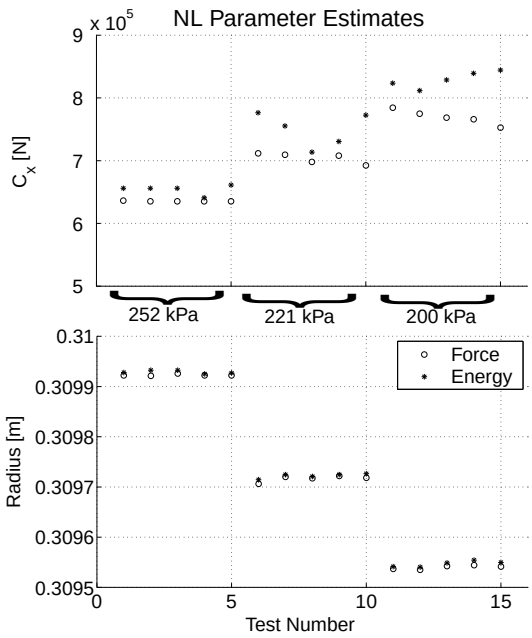

Figure 10: Stiffness and radius estimates for data taken at $252kPa$, $221[kPa]$ and $200[kPa]$ tire pressures

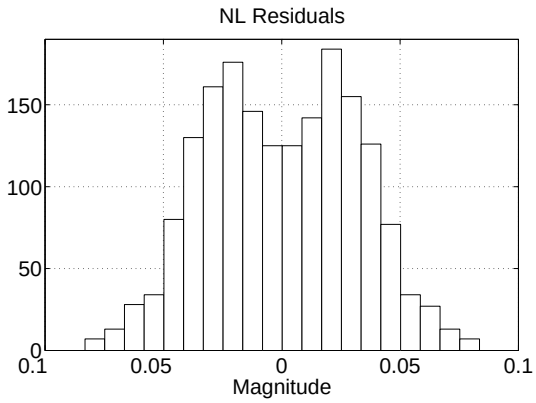

Figure 11: Typical bimodal residual histogram of force and energy estimation schemes

Potential sources of modeling error are numerous. Road grade, although probably small, is in reality not zero for the test site. The extra force term introduced by grade is unmodeled and may be biasing the results. In particular the energy form of the equation will tend to accumulate error due to road grade as the estimation scheme compares the total paths travelled by the front and rear wheels to the kinetic energy of the vehicle and ignores the change in potential energy.

Tire temperature is not monitored during the tests nor between tests. Particularly at lower pressures, the tires tend to heat and raise internal tire pressures by several psi. There may not have been adequate time for the tires to cool down in between tests which would change the longitudinal stiffness and effective radius from run to run. Additionally, tires heating up during the test will behave differently at the beginning than at the end. This variation of tire properties is not modeled and may tend to bias the results.

As mentioned in the nonlinear truth simulation section, the cost function for both estimators is extremely sensitive to wheel radius variation. Variation of the front wheel radius estimate on the order of $0.1[mm]$ could yield as much as a $2.5 \times 10^5[N]$ variation in the longitudinal stiffness estimate. During $3[m/s^2]$ accelerations, the front to back weight transfer of the test vehicle is at least $1.3 \times 10^3[N]$. This amount of force variation was measured using GPS velocity to yield about a $0.5[mm]$ change in free rolling radius at $13[m/s]$. This effect has not yet been modeled and may be introducing a bias as well, however, it is unlikely that the longitudinal stiffness estimates are off by several orders of magnitude. The free rolling radius is approximately linearly dependent on normal load which is varying cyclicly. Thus on average the free rolling radius of the tire is probably close to its steady state value.

6 FUTURE WORK

The Dynamic Design Lab is still actively researching models of tire-road interaction. It is known [12] that tire longitudinal stiffness exhibits a strong dependence on normal load. Current work recasts the problem to include this effect and seeks to quantify the influence of normal load variation due to weight transfer.

Recent work in [2] demonstrates the effectiveness of explicitly measuring road grade while estimating aerodynamic drag and rolling resistance. These proposed schemes could be used to correct the errors

associated with the flat surface assumption and provide a better estimate of the inertial forces during acceleration and braking.

In future tests tire pressure and temperature will be monitored in real time to account for tire pressure variation due to unmodeled factors such as frictional heating.

Once a consistent longitudinal stiffness model has been fully developed, data will be taken for different values of peak road friction in an effort to understand how low values of slip may be used for predicting the peak of the force-slip curve.

Many current vehicle navigation systems rely on the odometer and wheel effective radius to estimate position when a global position reference is unavailable [1, 5, 13]. Wheel slip during normal driving introduces significant errors to the position estimate. Future work will investigate how these schemes may benefit from modeling tire force-slip behavior.

7 CONCLUSION

Tire properties are complex and the measurement of slip characteristics is much more difficult that it first appears. A simulation study shows that even under idealized conditions, a linear regression with nonlinear measurements will yield significantly biased parameter estimates in two different formulations. However, by using iterative algorithms which seek to minimize measurement errors instead of equation errors, it is possible to achieve very good estimates of tire slip parameters using two different nonlinear estimation heuristics. These techniques applied to real data show that measured tire pressure and estimated longitudinal stiffness are approximately inversely proportional as noted by [12]. These results are encouraging, however the current model structure may be overly simple. Other effects such as road grade, tire temperature, and free rolling radius deformation may have significant impact on longitudinal stiffness estimates. Future work will study these unmodeled effects in more detail and quantify their influence on these parameter estimation schemes.

REFERENCES

[1] Eric Abbott and David Powell. Land Vehicle Navigation Using GPS. In *Proceedings of the IEEE*, volume 87, No. 1, pages 145–162, January 1999.

[2] H. S. Bae, J. Ryu, and J. C. Gerdes. Road Grade and Vehicle Parameter Estimation for Longitudinal Control Using GPS. In *IEEE Conference on Intelligent Transportation Systems, Proceedings, ITSC*, pages 166–171, 2001.

[3] E. Bakker, L. Nyborg, and H.B. Pacejka. Tyre Modelling for Use in Vehicle Dynamics Studies. In *SAE Paper*, 1987.

[4] Carlos Canudas-De-Wit and Roberto Horowitz. Observers for Tire/Road Contact Friction Using Only Wheel Angular Velocity Information. In *Proceedings of the* 38^{th} *Conference on Decision and Control*, pages 3932–3937, 1999.

[5] Christopher Robert Carlson, J. Christian Gerdes, and J. David Powell. Practical Position and Yaw Rate Estimation with GPS and Differential Wheelspeeds . In *Proceedings of AVEC 2002* 6^{th} *International Symposium of Advanced Vehicle Control*, 2002.

[6] David Bevly et al. The Use of GPS Based Velocity Measurements for Improved Vehicle State Estimation. In *Proceedings of the American Control Conference, Chicago IL*, pages 2538–2542, 2000.

[7] Paul Grygier, W. Riley Garrott, Elizabeth N. Mazzae, James D. MacIsaac Jr., Richard L. Hoover, Devin Elsasser, and Thomas A. Ranney. Examination of Existing Tire Pressure Monitoring Systems. *DOT HS 809 297*, 2001.

[8] Fredrik Gustafsson. Monitoring Tire-Road Friction Using The Wheel Slip. In *IEEE Control Systems Magazine*, pages 42–49, 1998.

[9] Wookug Hwang and Byung-Suk Song. Road Condition Monitoring System Using Tire-Road Friction Estimation. In *Proceedings of AVEC 2000* 5^{th} *International Symposium of Advanced Vehicle Control*, pages 84–89, 2000.

[10] Shannon L. Miller, Brett Youngberg, Alex Millie, Patrick Schweizer, and J. Christian Gerdes. Calculating Longitudinal Wheel Slip and Tire Parameters Using GPS Velocity. In *Proceedings of the American Controls Conference*, 2001.

[11] Laura Ray. Nonlinear Tire Force Estimation and Road Friction Identification, Simulation and Experiments. *Automatica*, 33, no. 10:1819–1833, 1997.

[12] H. Sakai. Theoretical and Experimental Studies on the Dynamic Properties of Tyres, part 4. *International Journal of Vehicle Design*, 3:333–375, 1982.

[13] J. Stephen and G. Lachapelle. Development and Testing of a GPS-Augmented Multi-Sensor Vehicle Navigation System. *The Journal of Navigation, Royal Institute of Navigation,*, 54, no. 2(May issue):297–319, 2001.